

Dynamical phenomena in sunspots

I. Time dependent relaxation to equilibrium

R.T. Gangadhara and S.S. Hasan

Indian Institute of Astrophysics, Bangalore – 560 034, India

Received 17 February 1997 / Accepted 29 May 1997

Abstract. We have adapted a general purpose time-dependent 2-D code to study dynamical phenomena in sunspots. In the first part of our investigation, we numerically simulate the dynamical relaxation to equilibrium of a sunspot. Treating the sunspot as a thick axisymmetric flux tube in cylindrical geometry, we solve the time dependent MHD equations to examine the evolution of a sunspot towards equilibrium, starting from an arbitrary initial state. Initially, we choose a potential magnetic field configuration and assume hydrostatic equilibrium along field lines, which allows the pressure variation along the field to be determined, for a known temperature distribution. We also assume that all quantities in the tube have a smooth and continuous radial variation. In particular the pressure increases radially from the tube axis to the photospheric value. The absence of Lorentz forces to balance the radial pressure gradient, leads to an inflow of gas towards the axis accompanied by an increase in the magnetic field strength. A complex flow pattern develops in the tube, which eventually dies out due to escape of matter upwards along the field lines. In the quasi-equilibrium state it is found that the field lines near the center of a large spot assume a configuration which is almost potential while those at the periphery depart significantly from the initial state, due to being pushed inwards by the gas flow. Our method is applicable to both thin and thick flux tubes. Further it can be readily extended to any coordinate system with 2 or 3 coordinates, and to discontinuous configurations such as current sheets. Forthcoming studies will focus on an extension of the present study to an analysis of dynamical effects in sunspots associated with nonlinear waves and examine the transport of energy by these to the corona.

Key words: magnetohydrodynamics – Sun: sunspots

1. Introduction

Sunspots are the sites of strong magnetic fields. They are generally associated with flux emergence at the solar surface and are

Send offprint requests to: S.S. Hasan

the best observed forms of structured fields in the form of thick flux tubes. Flux tubes are widely regarded as the fundamental building block of the photospheric magnetic field. Despite several observational and theoretical advances in sunspot physics, the basic processes that lead to the coolness of spots, their formation and equilibrium structure are not fully understood. The development of sunspot models has been hampered by the complexity of the MHD equations, which has imposed restrictions on the analytic and numerical solutions that can be obtained.

Theoretical models developed so far treat the equilibrium of a sunspot as a 2-dimensional structure extending vertically through the photosphere. Some of the basic characteristics of the flux tube behavior are explained by such models, even though they unrealistically treat the momentum balance equation in isolation, without taking into account the energy balance. Another assumption that has often been invoked is the thin flux tube approximation (e.g., Defouw 1976; Roberts & Webb 1978), which works well for small-scale flux tubes, but is inappropriate for thick flux tubes, such as pores and sunspots. This is because the horizontal dimensions of these tubes are typically many times the atmospheric scale height. Solutions for thick flux have been obtained under various approximations.

The earliest quantitative model for sunspots was developed by Schlüter & Temesváry (1958), based upon a *similarity assumption*, in which the stratification and field geometry are specified. This work was extended by Deinzer (1965), Yun (1970, 1971), Solov'ev (1982, 1983), Jakimiec (1965), Jakimiec & Zabža (1966), Landman & Finn (1979), and Low (1980). Return flux models which allow the magnetic field lines to re-enter the solar surface just outside the spot are a further development of the similarity assumption (Skumanich & Osherovich 1981; Osherovich 1982; Osherovich & Flá 1983; Osherovich & Lawrence 1983). In recent years, the solution of the magnetostatic equations has broadly followed two approaches: direct solution of the partial differential equations, and free surface problem.

In the first class of solutions, the earlier models assumed a continuous variation of the magnetic field across the spot. Here the separation between the internal and external regions is not sharply defined; rather the magnetic field is assumed to fall

smoothly from a maximum at the axis to zero at some large radial distance. Based upon this assumption, magnetostatic equilibria were constructed by Pizzo (1986). The inclusion of a sharp interface between the sunspot and ambient medium in the form of a current sheet was treated amongst others by Simon & Weiss (1970), Meyer et al. (1977), Simon et al. (1983), and Pizzo (1990).

In the second approach, the direct solution of the equilibrium force balance equation is replaced by a free surface problem over which the total pressure, which is the sum of the gas and magnetic pressures, is continuous across the current sheet. Such models have been constructed for example by Schmidt & Wegemann (1983), and Jahn (1989).

All the above mentioned models are somewhat restrictive and describe a subset of the family of equilibrium solutions. Furthermore, they assume a static situation from the beginning, which may be a limitation. Also, it is well known that sunspots are not truly static structures but evolve with time. In order to model this evolution, we need to solve the time dependent MHD equations. There are numerous time dependent studies of thick flux tubes such as those carried out in 2-D by Deinzer et al. (1984a,b), Grossmann Doerth et al. (1989, 1994), Knölker et al. (1991), Steiner et al. (1994) and in 3-D by Nordlund & Stein (1989, 1990). These elaborate studies have contributed significantly to understanding the nature of flux tubes and also to model the interaction of convection with magnetic fields. For example, the work by Nordlund & Stein (1989, 1990) considers the interaction of granulation with a strong vertical magnetic field and shows that the latter suppresses the convective transport of energy leading to a cooling of the atmosphere which may simulate umbra formation in a sunspot. In the present investigation we adopt a somewhat different approach. Starting from a potential field configuration, which is clearly not in dynamical equilibrium, we attempt to examine whether the temporal evolution of this state can lead to an equilibrium solution which for instance is similar to the solutions computed using the magnetostatic equations. Cooling effects due to the reduced convective transport in the sunspot will not be considered in this study and are deferred to a future investigation. The main focus of this work is to use a viable numerical technique for modeling dynamic phenomena in sunspots. In the first part of this study, we apply this method to examine the time dependent relaxation of a potential field. In subsequent papers, we hope to extend our calculations to study dynamic behaviour in sunspots associated with wave motions, Evershed flows and non-adiabatic effects involving radiative energy transport.

We present a numerical simulation for the equilibrium configuration of a sunspot starting from an arbitrary initial state using dynamic relaxation. For the purposes of this investigation, we work within the framework of a distributed magnetic field configuration, deferring the treatment of a current sheet to a subsequent paper. The computational method is based on ZEUS-2D, a code for solving the MHD equations in 2-D (Stone & Norman 1992a, 1992b). We present in Sect. 2 the MHD equations, written in a form which lends itself naturally to conservation of the physical variables. In Sect. 3, we discuss the ini-

tial state, which corresponds to a potential magnetic field over the computational domain. Next, we point out the initialization and boundary conditions for the MHD variables. The results of our numerical simulation are presented in Sect. 4. Finally, we discuss the significance of the results and outline future work Sect. 5.

2. MHD Equations and strong form of conservation laws

The non-relativistic MHD equations for a perfectly conducting fluid are

$$\frac{D\rho}{Dt} + \rho \nabla \cdot \mathbf{v} = 0, \quad (1)$$

$$\rho \frac{D\mathbf{v}}{Dt} = -\nabla p - \rho \mathbf{g} + \frac{1}{c} \mathbf{j} \times \mathbf{B}, \quad (2)$$

$$\rho \frac{D}{Dt} \left(\frac{e}{\rho} \right) = -p \nabla \cdot \mathbf{v}, \quad (3)$$

$$\frac{\partial \mathbf{B}}{\partial t} = \nabla \times (\mathbf{v} \times \mathbf{B}), \quad (4)$$

where ρ , e and \mathbf{v} are the fluid density, internal energy density and velocity, respectively; \mathbf{B} is the magnetic flux density, and \mathbf{g} is the acceleration due to gravity of the Sun. The factor $\frac{D}{Dt}$ denotes the Lagrangian or convective derivative. The current density \mathbf{j} is related to \mathbf{B} by

$$\frac{4\pi}{c} \mathbf{j} = \nabla \times \mathbf{B}. \quad (5)$$

The fluid equations are closed by an equation of state $p = p(\rho, e)$.

Eqs. (1)–(3) describe the conservation of mass, momentum and energy, and Eq. (4) is the induction equation which is a re-statement of magnetic flux conservation. In order to minimize truncation errors associated with finite differencing, it is convenient to recast the above equations in strong conservation form, which may be derived by integrating Eqs. (1)–(4) over an arbitrary control volume and its surface. This control volume corresponds to an individual cell or zone, in the desired spatial grid.

Consider a moving finite control volume $V(t)$ with surface $S(t)$. Using the adaptive grid transport theorem (Winkler et al. 1984), the integration of Eqs. (1)–(3), yields

$$\frac{d}{dt} \int_V \rho dV = - \oint_s \rho (\mathbf{v} - \mathbf{v}_g) \cdot d\mathbf{S}, \quad (6)$$

$$\begin{aligned} \frac{d}{dt} \int_V \rho \mathbf{v} dV = & - \oint_s \rho \mathbf{v} (\mathbf{v} - \mathbf{v}_g) \cdot d\mathbf{S} - \\ & \int_V (\nabla p + \rho \mathbf{g} - \frac{1}{c} \mathbf{j} \times \mathbf{B}) dV, \end{aligned} \quad (7)$$

$$\frac{d}{dt} \int_V e dV = - \oint_s e (\mathbf{v} - \mathbf{v}_g) \cdot d\mathbf{S} - \int_V p (\nabla \cdot \mathbf{v}) dV, \quad (8)$$

where \mathbf{v}_g is the grid velocity measured with respect to the Eulerian frame. The factor $\frac{d}{dt}$ denotes the total derivative with respect to the moving frame

$$\frac{d}{dt} \equiv \frac{\partial}{\partial t} + \mathbf{v}_g \cdot \nabla. \quad (9)$$

Similarly, integrating Eq. (4) over a moving surface element $S(t)$ bounded by a moving circuit $C(t)$, one derives the general form of Faraday's law (Jackson 1975),

$$\frac{d}{dt} \int_S \mathbf{B} \cdot d\mathbf{S} = \oint_C (\mathbf{v} - \mathbf{v}_g) \times \mathbf{B} \cdot d\mathbf{l}. \quad (10)$$

The ZEUS-2D solves the MHD equations using an explicit, multistep (operator split) finite difference method, the details can be found in the papers of Stone & Norman (1992a, b). However, for the sake of completeness we briefly mention the salient features of the algorithm. The fluid Eqs. (6)–(8) are solved in two steps, called the *source* and *transport* steps. In the source step, the following equations are solved in finite difference form

$$\rho \frac{\partial \mathbf{v}}{\partial t} = -(\nabla p + \rho \mathbf{g}) - \nabla \cdot \mathbf{Q} + \frac{1}{c} \mathbf{j} \times \mathbf{B}, \quad (11)$$

$$\rho \frac{\partial e}{\partial t} = -p \nabla \cdot \mathbf{v} - \mathbf{Q} : \nabla \mathbf{v}, \quad (12)$$

where the volume integration is dropped and an artificial viscous stress tensor \mathbf{Q} has been introduced to treat shock waves. Next, in the transport step, the advection of fluid and magnetic flux is treated by solving

$$\frac{d}{dt} \int_V \rho dV = - \oint_S \rho (\mathbf{v} - \mathbf{v}_g) \cdot d\mathbf{S}, \quad (13)$$

$$\frac{d}{dt} \int_V \rho \mathbf{v} dV = - \oint_S \rho \mathbf{v} (\mathbf{v} - \mathbf{v}_g) \cdot d\mathbf{S}, \quad (14)$$

$$\frac{d}{dt} \int_V e dV = - \oint_S e (\mathbf{v} - \mathbf{v}_g) \cdot d\mathbf{S}, \quad (15)$$

$$\frac{d}{dt} \int_S \mathbf{B} \cdot d\mathbf{S} = \oint_C (\mathbf{v} - \mathbf{v}_g) \times \mathbf{B} \cdot d\mathbf{l}. \quad (16)$$

We solve the finite-difference equations by expressing them in covariant form in a cylindrical coordinate system. We ignore the azimuthal coordinate since we assume axial symmetry. This reduces the number of independent variables to two, while all components of vectors and tensors are retained. This approach is sometimes referred to as MHD in 2.5D.

The constraint that the magnetic field remain divergence free is implemented in the numerical treatment using the constrained transport (CT) algorithm of Evans & Hawley (1988). This is achieved by using the integral formulation of the induction equation to evolve the magnetic flux (Eq. 16). In addition it is important to calculate the EMF ($\mathbf{v} \times \mathbf{B}$) accurately and in a manner which ensures numerical stability. The manner in which this is implemented in the code is described in Stone & Norman (1992b).

3. Initial configuration

3.1. Initialization of the magnetic field

Let us consider an initial configuration which is static (i.e. without flows) and one in which the magnetic field varies smoothly in the radial direction. In cylindrical geometry the magnetic field for an axisymmetric configuration can be expressed, following Low (1975), in terms of the field line constant u and vector potential $\mathbf{A} = A \hat{\phi}$, as $u = Ar$, where r is the radial distance from the flux tube axis. The pressure can be determined in terms of u , which is initially unknown. We specify u by choosing a potential field at the initial epoch — clearly not an equilibrium solution. We evolve this configuration in time to see whether a final equilibrium state results.

Let us consider a cross section of the flux tube in a rectangular domain of the r - z plane, and initialize the magnetic field on all the grid points using the potential solution, i.e., the solution of the equation (Low 1975)

$$\nabla^2 u = \frac{\partial^2 u}{\partial r^2} - \frac{1}{r} \frac{\partial u}{\partial r} + \frac{\partial^2 u}{\partial z^2} = 0. \quad (17)$$

Let us choose the flux tube axis to be at $r = 0$ and its base at $z = 0$. The level $z = 0$ at this stage is somewhat arbitrary, since we have yet not specified its location with respect to the photosphere in the quiet atmosphere. At $r = 0$, we assume that the field \mathbf{B} is vertical along the axis and the field line constant $u = 0$. The latter involves no loss of generality as it the gradient of u that matters. Since we assume axial symmetry, the field lines cannot cross the axis of the flux tube. Along the lower boundary ($z = 0$), a Dirichlet boundary condition is used by specifying the vertical magnetic field B_z . On the top ($z = z_1$) and side ($r = r_1$) surfaces, we use Neumann boundary conditions (normal derivative set to zero) similar to Pizzo (1986).

Following Pizzo (1986), we assume a Gaussian variation of B_z along the base of the flux tube

$$B_z(r, z = 0) = B_0 \exp\{-(r/r_e)^2\}, \quad (18)$$

where B_0 is the axial field strength at $r = 0$, and r_e is the e-folding distance.

The components of the magnetic field in terms of the field line constant u are:

$$B_r = -\frac{1}{r} \frac{\partial u}{\partial z}, \quad (19)$$

$$B_\phi = 0, \quad (20)$$

$$B_z = \frac{1}{r} \frac{\partial u}{\partial r}. \quad (21)$$

Using Eqs. (18) and (21), the field line constant u along $z = 0$ is generated,

$$u(r, z = 0) = \frac{B_0 r_e^2}{2} [1 - \exp\{-(r/r_e)^2\}]. \quad (22)$$

At large radial distance from the axis, B_z approaches zero while u approaches a constant value $u_1 = B_0 r_e^2 / 2$, in accordance with

Neumann boundary conditions, assumed on the outer boundaries. Along $r = 0$, i.e., along the axis of the flux tube, the axisymmetry is used to specify the magnetic field.

Using $B_0 = 2$ kG, $r_e = 3$ Mm, $r_1 = 20$ Mm and $z_1 = 12$ Mm, the potential solution of Eq. (17) is computed using the Cyclic Reduction Algorithm (CRA) developed by Swarztrauber (1974, 1977). Fig. 1 shows the contours of the field line constant u . We use this solution to calculate the magnetic field over the computational domain in the r - z plane and thereby initiate the numerical simulation.

3.2. Initialization of the hydrodynamic variables

From observations it is well known that sunspots are cool and possess a pressure that is less than that of the ambient photosphere. The decrease of the pressure with height, leads to a fanning out of the magnetic field lines with height. For a axisymmetric and vertical flux tube in magnetostatic equilibrium, Low (1975) has shown that the gas pressure variation along a field line has the form

$$p(u, z) = p_0(u) \exp \left[- \int_0^z \frac{dz'}{h(u, z')} \right], \quad (23)$$

where $p_0(u)$ is the gas pressure along the lower boundary ($z = 0$) and h , the isothermal scale height along a field line, is

$$h = \frac{p}{\rho g}. \quad (24)$$

For a perfect gas, the temperature T can be related to h as follows

$$h = \frac{RT}{\mu g}, \quad (25)$$

where μ is the mean molecular weight, and $R = 8.3145 \times 10^7$ erg/deg-mol is the universal gas constant.

Given $p_0(u)$ and $h(u, z)$, $p(u, z)$ can be specified over all the grid points in the r - z plane. The temperature can be found from Eq. (25) and the density is readily obtained using the perfect gas law. The components of the magnetic field have already been computed using the potential solution based on Eq. (17). Thus, in principle, we have the necessary information to solve the initial value MHD problem, subject to some choice of boundary conditions. It should be pointed out that the pressure and magnetic field distributions chosen in this way are not self-consistent, since the magnetic field is in general not potential. However, we follow this procedure only to specify the initial values of the variables.

For our model sunspot simulations, we require a representative umbral atmosphere along the axis and a quiet photospheric atmosphere at large horizontal distances, where the field vanishes. For thick flux tubes with a distributed current, we construct a smooth transition between the quiet photospheric atmosphere and the sunspot. Following Pizzo (1986), we extract the values at the base using a smooth transition from the sunspot-sunspot model of Avrett (1981) on the axis to the convection

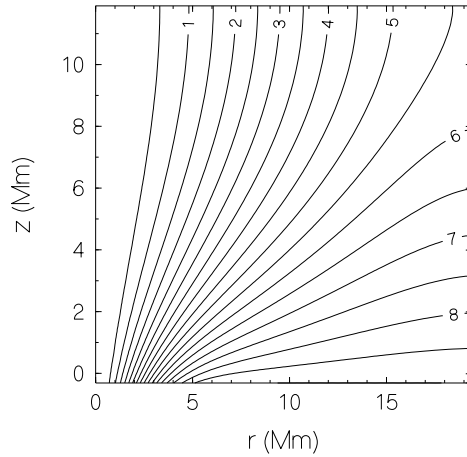


Fig. 1. Magnetic field topology for the potential solution, computed over a rectangular domain in the r - z plane, assuming that the field lines intersect the outer ($r = 20$ Mm) and upper ($z = 12$ Mm) boundaries normally. This solution is used to specify the magnetic field at the initial stage of the simulation. The labels on contours indicate the values of u in units of (kG Mm^2)

model of Spruit (1977) for the quiet photosphere. The location of our base is chosen similar to Pizzo (1986) to lie at a depth of 120 km (i.e. below continuum optical depth unity) in the sunspot-sunspot model, which is displaced relative to the photosphere by the Wilson depression (i.e., the level corresponding to which the continuum optical depth in the vertical direction is unity). This is the $z = 0$ level in our model. Let $p_{int}(z = 0) = p_b(0)$ be the umbral gas pressure at $z = 0$ based on the sunspot-sunspot model. At the equivalent geometric depth, let the gas pressure in the quiet photosphere model be $p_{ext}(z = 0) = p_b(u_1)$.

We now consider a smooth transition of the pressure from the axis to the exterior, chosen in such a way that it has the same functional dependence on u as B_z^2 . Using Eqs. (18) and (22), we obtain $B_z(r, z = 0) \approx B_o(1 - u/u_1)$. The rate of increase of $p_{int}(z = 0)$ to $p_{ext}(z = 0)$ matches with the decrease of B_z^2 if

$$p_b(u) = p_b(u_1) - [p_b(u_1) - p_b(0)] \left(1 - \frac{u}{u_1} \right)^2. \quad (26)$$

For $p_{int}(z = 0) \equiv p_b(0) = 6 \times 10^4$ dyne cm^{-2} and $p_{ext}(z = 0) \equiv p_b(u_1) = 1.35 \times 10^6$ dyne cm^{-2} , we find

$$\begin{aligned} \frac{p_b(u)}{B_o^2/8\pi} &= 8.5 - 4.7 \left(1 - \frac{u}{u_1} \right)^2 \\ &= 8.5 - 4.7 \exp[-2r^2/r_e^2]. \end{aligned} \quad (27)$$

It shows that the gas pressure increases sharply from the axis to $r = r_e$, after which it becomes almost constant.

We now need to specify the variation of $h(u, z)$. For simplicity, we assume that h is independent of z , and take the following dependence with respect to u ,

$$h(u) = h_{ext}(0) - [h_{ext}(0) - h_{int}(0)] \left(1 - \frac{u}{u_1} \right)^2. \quad (28)$$

Table 1. Basic parameters for the prototype solution

Step 1	Step 2
$B_o = 2 \text{ kG}$	WD = 500 km
$r_e = 3 \text{ Mm}$	$\log_{10} P_{int}(\text{dyne cm}^{-2}) = 5.78$
$z_1 = 10 \text{ Mm}$	$\log_{10} P_{ext}(\text{dyne cm}^{-2}) = 6.13$
$r_1 = 20 \text{ Mm}$	$h_{int} = 162 \text{ km}$
	$h_{ext} = 365 \text{ km}$
	$\log_{10} \rho_{int}(\text{g cm}^{-3}) = -5.87$
	$\log_{10} \rho_{ext}(\text{g cm}^{-3}) = -5.86$

The functional dependence of p_b and h on u in Eqs. (26)–(28) are the same as those used by Pizzo (1986). We choose $h_{int} = 162 \text{ km}$ and $h_{ext} = 365 \text{ km}$, which correspond to temperatures on the axis and in the ambient medium of $6.9 \times 10^3 \text{ K}$ and $1.5 \times 10^4 \text{ K}$ respectively, assuming $\mu = 1.3$.

The pressure along a field line can now be calculated using Eq. (23). This pressure distribution is at best an approximation to the magnetostatic solution and as already stated is used only to initiate the simulation. From a practical point of view, it is more convenient to calculate the pressure from Eq. (23), assuming that the field lines are *straight*. Clearly, the surfaces of constant u do not coincide with surfaces of constant r , but we make this assumption only to specify the starting value of p , since the final equilibrium state is unlikely to depend upon the precise values of the variables at the initial instant of time.

4. Numerical solutions for a prototype model

In this paper we concentrate on a single set of parameters characterizing our initial state, which define a prototype sunspot model. These are shown in Table 1 and are taken from Pizzo (1986).

4.1. Boundary conditions

For the time-dependent simulation we consider a computational region in the $r - z$ plane, with lower and upper boundaries at $z = 0$ and $z = 1 \text{ Mm}$ respectively. In the radial direction the boundaries are taken at $r = 0$ and $r = 4 \text{ Mm}$. At the base ($z = 0$) and on the axis ($r = 0$), we assume no flow through boundary conditions. The choice of a no flow boundary through condition at the base can be justified to some extent on the basis of the high density of matter, which plays the role of an impenetrable boundary. The assumption of axial symmetry precludes gas flow across the axis of the sunspot. On the right boundary, we allow for an inflow boundary condition. This is to be expected on physical grounds as a consequence of the horizontal pressure difference between the interior and exterior of the sunspot. We allow for the escape of matter along field lines from the upper boundary, where we use an outflow boundary condition.

The ZEUS code utilizes two rows of ‘ghost’ zones at each boundary. The boundary conditions ensure that the values stored

in the ghost zones are consistent with the active zones. Boundary conditions are used to update the values of the thermodynamics variables (p , ρ and e), the velocity and the EMF (the actual values of the magnetic field components can be found from the difference equations). At the base and on the axis, we use reflecting boundary conditions. These equate the thermodynamic variables and the tangential velocity in the ghost zones to the values of these variables in their active zone images. The normal components of velocity and magnetic field are reflected, which implies that the EMF in a ghost zone is negative of the value in the active zone image. Actually, for the ghost zones parallel to the axis, we need to also reflect the azimuthal component of the velocity in view of the symmetry. In the present case, however, this is inapplicable since we assume that the flow does not possess an azimuthal component.

Having initialized all the magnetohydrodynamic variables, we numerically solve the MHD equations as a time dependent problem with the goal of achieving an equilibrium configuration for a sunspot.

4.2. Flow pattern in the sunspot

At $t = 0$ the fluid velocity over the entire mesh is set to zero. However, the initial state is clearly not in equilibrium. Thus, as soon as the simulation begins, we expect that the negative horizontal pressure gradient will lead to a radial inflow of matter from the right boundary. Let us first examine the nature of the flow pattern that is set up in the sunspot.

Fig. 2a–h, depict the velocity (flow) field in the computational domain as a vector plot at different instants of time. The length of the arrows, drawn at random points, is proportional to the magnitude of the velocity, whereas their orientation indicates the direction of the flow. The normalization in each panel is with respect to the largest value of the flow at that instant of time.

Fig. 2a shows the flow field at time $t = 6.3 \text{ s}$, which is radially inward due to the gradients in pressure and density. The length of the arrow having maximum length is $\sim 10^3 \text{ m s}^{-1}$, and all other vectors are normalized with this length. Initially, the horizontal pressure gradient leads to a radial inflow of matter. Since this matter cannot flow out through the axis in view of our assumption of axial symmetry, the fluid density increases near the axis. The increase in density leads to a downflow of matter due to gravity towards the base of the flux tube. This can be discerned in Figs. 2b and c. Since we have assumed an impenetrable boundary at the base, there is an accumulation of fluid near the base, which results in a pressure buildup there. This leads to a reversal of the flow in the vertical direction, as can be seen in Fig. 2d for $t = 127 \text{ s}$. The depletion of fluid from near the base along with magnetic tension forces result in fluid again moving downward as indicated by Fig. 2e at $t = 255 \text{ s}$. This pattern of flow reverses in time. Over each cycle the absolute value of the velocity decreases in magnitude, due to the gradual diminution of the pressure, gravitation and Lorentz forces, driving the flow. This is accompanied by a escape of matter along the field lines through the upward boundary. Fig. 2f–h display the

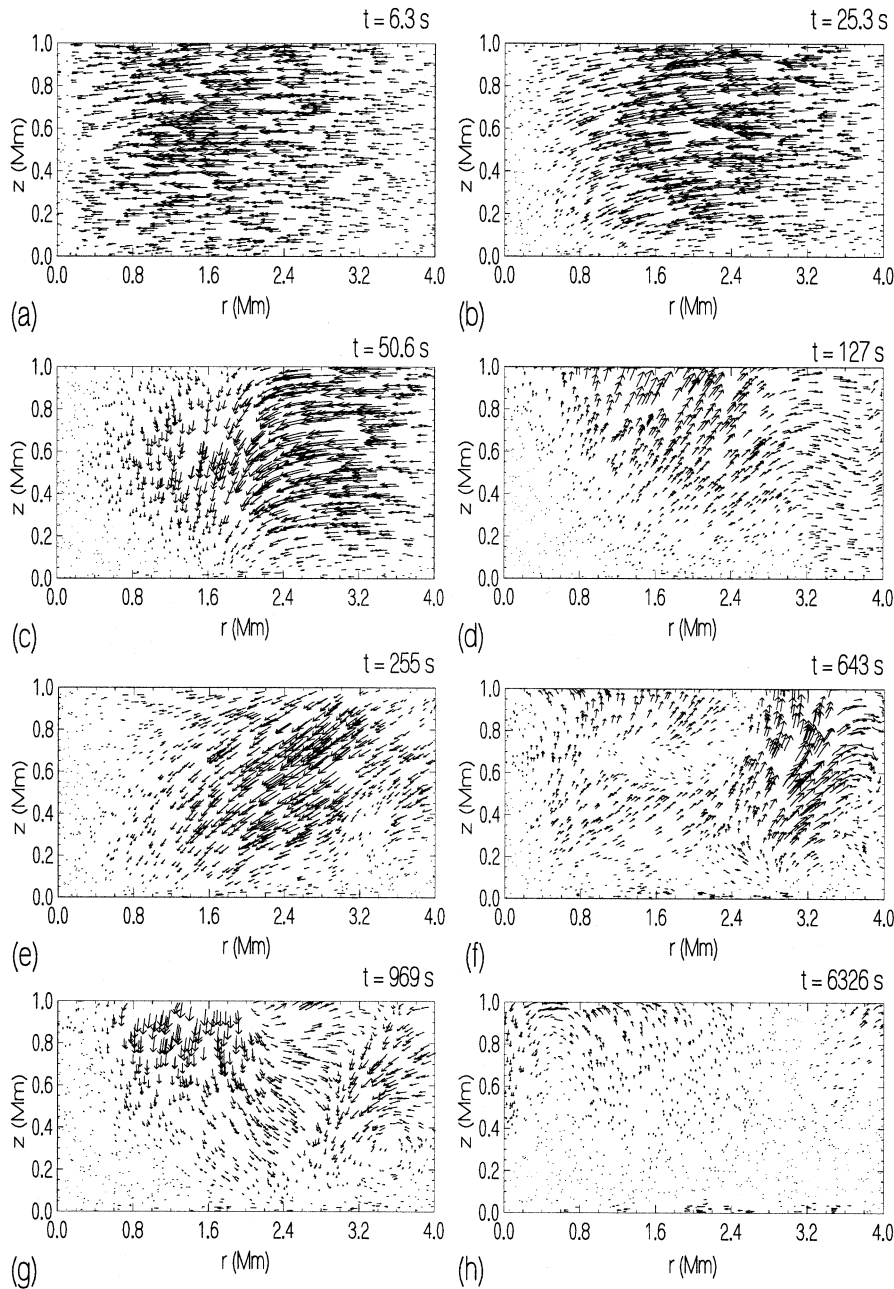


Fig. 2a–h. Series of vector fields for fluid velocity in the $r-z$ plane at various instants of time during the simulation. The size of the computation domain selected in the simulation is 4 Mm in the r -direction and 1 Mm in z -direction. The length and direction of arrows indicate the magnitude and direction of fluid velocity at different regions over the computation domain: **a** gas flow towards the axis of the flux tube due to pressure and density gradients, **b** and **c** flow towards the base due to gravity, **d** reflection of the flow due to the impenetrable lower boundary and the instantaneous generation of high pressure and density near the base and axis, **e** fluid comes back due to gravity and tension forces in the magnetic field lines

flow field direction at subsequent times. It may be noted that the arrows lengths decrease in time. In Fig. 2h, the absolute value of the maximum velocity at $t=6326$ s is about 100 m s^{-1} , which is very much less than the sound and Alfvén speeds, typically in the range of ten to hundred km s^{-1} .

4.3. Field line topology

Fig. 3 depicts the geometry of the magnetic field at $t=0$ s (dashed lines) and at $t=6326$ s (continuous lines). The curves are labeled by the constant u , along the field. The initial geometry of course corresponds to the potential field solution. We find that the field lines are compressed relative to the potential field

and tends to become more vertical owing to the squeezing action due to the radial inflow. Fig. 4 shows contours of constant field (in kilogauss) for the initial (dashed lines) and asymptotic (solid lines) solutions. Close to the axis of the field, we can clearly discern that the contours get shifted upwards, which as already mentioned is a consequence of field compression due to the flow. The heavy dashed and solid lines denote the $\beta = 1$ levels at the initial and final instants respectively, where $\beta = 8\pi p/B^2$. The significance of these curves is that they delineate the boundary in the flux tube between the regions where pressure and magnetic forces dominate. The Lorentz forces are more important in controlling the momentum balance in the spot atmosphere above these curves (where $\beta \ll 1$), whereas in the underlying

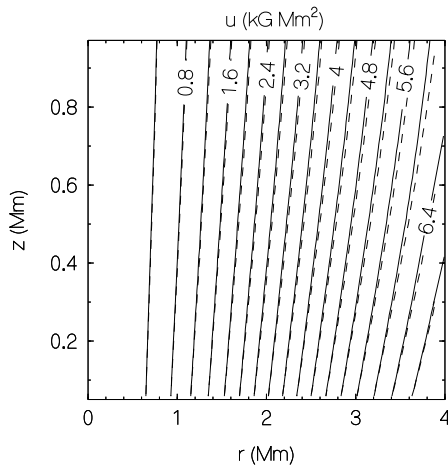


Fig. 3. Field lines for the final (continuous lines) and initial potential field (broken lines) states. Labels indicate the constant value of u along each field line. Note that in the final state, the field lines are pushed inwards towards the axis with respect to the potential field

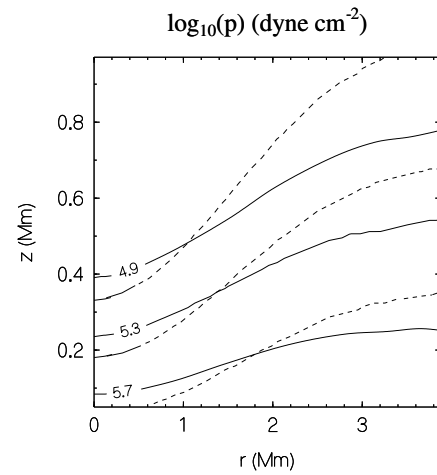


Fig. 5. Contours of constant $\log_{10}p$ in the final (continuous lines) and initial (broken lines) stages. Close to the axis there is an enhancement of the pressure, whereas away from the axis there is a decrease in pressure

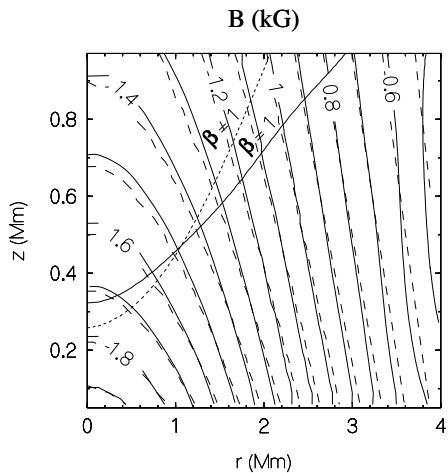


Fig. 4. Contours of constant B in the final (continuous lines) and initial (broken lines) stages. In the final stage, the magnetic field near the axis is lifted up by the gas while near the base it is pushed down. The heavy dashed and solid lines denote the $\beta = 1$ levels at the initial and final instants respectively, where $\beta = 8\pi\rho/B^2$

layers pressure forces are more significant. Near the axis, the $\beta = 1$ level is raised upwards, but at about a radial distance of 1 Mm from the axis, the level has been shifted downwards as a consequence of the flow. This indicates that the region where magnetic forces are important (essentially the area above the $\beta = 1$ curve) has become much larger as a consequence of the field enhancement.

4.4. Thermodynamic structure of the sunspot

Figs. 5 show contours of constant $\log_{10}p$ in the spot at the initial and final instants (in the asymptotic time limit the pressure is practically constant with time). Close to the axis the contours are shifted up, whereas away from the axis they are moved downwards. The relaxation of the spot under the large radial

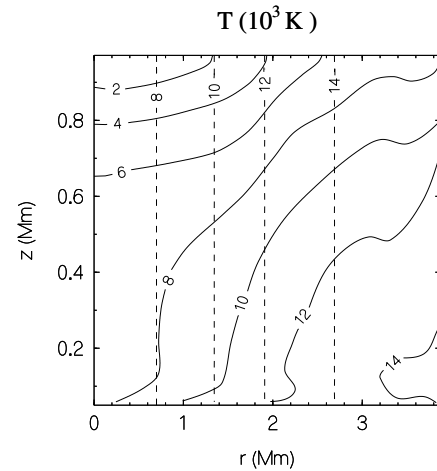


Fig. 6. Contours of constant temperature (in units of 10^3 K). Initially the isotherms are vertical (dashed lines). In the final state (solid lines), the isotherms are not so steep

pressure gradient at the initial instant leads to a diminution of this gradient in the final state. This is consistent with a decrease in pressure at large radial distances, whereas close to the axis, there is a slight increase in pressure (we rule out flow of matter across the spot axis). In the vertical direction, the state of hydrostatic equilibrium is almost restored after long enough time, when the flow has become very small.

Let us now consider the temperature structure in the sunspot, which is depicted in Fig. 6. At $t = 0$, we have assumed that the pressure scale height h and hence the temperature T vary only in the radial direction. Initially the isotherms, by assumption, are vertical (dashed lines) parallel to the axis of the tube. The curves are labeled by the constant value of temperature (in units of 1000 K). However, as the flux tube relaxes dynamically the scale height in general decreases upwards, resulting in a drop of temperature with height. This behaviour is equivalent to the statement that the temperature reduction is due to a decrease

in the internal energy per unit mass ($\sim p/\rho$). The isotherms become less steep and the temperature in the sunspot has a form which is closer to reality, viz., that the isotherms from the external atmosphere dip downwards into the spot. At equal geometric levels the temperature in the sunspot is less than that in the ambient medium.

5. Discussion

We should point out that the aim of this study is not to present a realistic model for a sunspot, but rather to demonstrate that a sunspot-like configuration can develop through the dynamic relaxation of a potential field configuration under the action of pressure forces. Earlier work by Pizzo (1986) had indicated that one can iteratively construct a magnetostatic equilibrium solution, by relaxing a potential field configuration through a sequence of equilibria. There are, however, two assumptions which are inherent in this procedure which need to be checked, viz. whether the different equilibrium solutions are in fact connected and secondly whether flows can be neglected. These assumptions can be verified by solving the time dependent equations which permit one to see the dynamical evolution of the potential field solution. Our simulation indeed shows, that a quasi-equilibrium state can be achieved, which is roughly similar to the configuration computed by Pizzo (1986) and one in which flows are small in the asymptotic time limit. An interesting feature of our simulation is the development of transient flows, which have a peak value of about 1.5 km s^{-1} . These flow gradually diminish and after long enough time become vanishingly small. This asymptotic state can be regarded as the *final equilibrium* solution, in which all quantities are constant with time.

In the present calculation we have assumed a smooth radial distribution of the magnetic field. Observations of pores (e.g., Steshenko 1967) and the similarity in flux distribution of most umbrae (Gokhale & Zwaan 1972) support the current sheet models, which allow for a sharp transition between the sunspot and quiet photosphere. Although this feature is absent in our model, we doubt whether its presence would change the essential nature of our results. Furthermore, the inclusion of a current sheet would involve major modifications to the ZEUS-2D package, which we defer to a later calculation.

In our analysis we have considered the lower boundary above the superadiabatic temperature layer. The reason for this is not because we believe that the influence of this layer is unimportant, but rather we expect that if the magnetic field is sufficiently strong, which is the case in these calculations, then the convective instability associated with the superadiabatic layer would be suppressed by the strong magnetic field. Indeed earlier studies on magneto-convection based on the Boussinesq approximation by Galloway & Moore (1979), and Weiss (1981 a,b) (additional references can be found for example in the review by Proctor 1992) have shown that convection in the presence of a vertical magnetic field leads to a sweeping of the field to the cell boundaries and to a realignment of the field lines in such a way as to minimize their interference to the convective motions. Thus,

the spot can be regarded as the region characterized by a strong vertical field and with significantly reduced convection. It is, however, well known that in certain cases oscillatory convection with motions essentially aligned with the vertical field can continue to exist, no matter how strong the field (Syrovatskii & Zhughzda 1967). For further details the reader can consult the papers by Proctor & Weiss (1982), Knobloch & Proctor (1981) and Hurlburt et al. (1989). Our aim in this work is to examine the dynamical motions that arise in the photospheric and chromospheric regions of sunspots where nonlinear effects may become important. We expect to incorporate, in subsequent papers, the oscillatory motions present in the convection zone through their buffeting action on the lower boundary in our problem.

A more important physical effect that has been neglected in the present work is the inclusion of a realistic energy equation which takes into account radiative and convective transport. It is well known (e.g., Spruit 1977) that radiation plays a significant role in the energy balance of flux tubes, particularly in the photospheric layers. Furthermore, the suppression of convection by the strong magnetic field and its effect on the thermodynamic structure of a spot also has not been treated by us, but which has been taken into account for instance by Nordlund & Stein (1989, 1990). However, we expect to consider this refinement in a subsequent paper of this series by incorporating an energy equation in the analysis.

This study marks the beginning of an investigation into various time dependent processes in thick flux tubes, such as sunspots, pores etc. It is well known from observations that such flux tubes are not static, but evolve and decay in time. Furthermore, they support a variety of wave motions, which are likely to be nonlinear in the upper layers of the solar atmosphere. In order to model these phenomena, an effective method is needed for solving the nonlinear time dependent MHD equations in multi-dimensions. We have developed such a method, based upon the ZEUS-2D algorithm, for modeling dynamical phenomena in sunspot-like configurations. The results indicate that our approach is robust and can be successfully applied to simulate the temporal evolution of a thick stratified flux tube. In subsequent papers, we shall enlarge the scope of the study to treat oscillations and their interaction with external wave modes, radiative transfer and their effect on the thermal structure, current sheets and ultimately the birth and decay of spots.

Acknowledgements. The authors are grateful to M. L. Norman, J. M. Stone and D. A. Clarke for providing them with the ZEUS-2D package. They are especially indebted to R. Fiedler for his help in implementing the code. The cyclic reduction algorithm was provided by P. Swartrauber. Thanks are also due to V. Pizzo for several illuminating discussions.

References

- Avrett E. H., 1981, in: *The Physics of Sunspots*, ed. L. E. Cram and J. H. Thomas (Sunspot: Sacramento Peak Observatory), p. 235
- Defouw R. J., 1976, *ApJ*, 384, 348
- Deinzer W., 1965, *ApJ*, 141, 548
- Deinzer W., Hensler G, Schüssler M., Weisshaar E., 1984a/b, *A&A*, 39, 426/435

- Evans C. R., Hawley J. F., 1988, *ApJ*, 332, 659
- Galloway D. J., Moore D., 1979, *Geophys. Astrophys. Fluid Dyn.*, 12, 73
- Gokhale M. H., Zwaan C., 1972, *Solar Phys.*, 26, 52
- Grossmann-Doerth U., Knölker M., Schüssler M., Weisshaar E. A., 1989, in: *Solar and Stellar Granulation*, Ed. R. J. Rutten & G. Severino (Dordrecht: Kluwer), p. 481
- Grossmann-Doerth U., Knölker M., Schüssler M., Solanki S. K., 1994, *A & A* 285, 648
- Hurlburt N. E., Proctor M. R. E., Weiss N. O., Brownjohn D. P., 1989, *J. Fluid Mech.*, 209, 587
- Jackson J. D., 1975, *Classical Electrodynamics*, New York: Wiley
- Jahn K., 1989, *A & A*, 222, 264
- Jakimiec J., 1965, *Acta Astr.*, 15, 145
- Jakimiec J., Zabza M., 1966, *Acta Astr.*, 16, 73
- Knobloch E., Proctor M. R. E., 1981, *J. Fluid Mech.*, 108, 291
- Knölker M., Grossmann-Doerth U., Schüssler M., Weisshaar, E., 1991, *Adv. Space Res.* 11, 285
- Landman D. A., Finn G. D., 1979, *Solar Phys.*, 63, 221
- Low B. C., 1975, *ApJ*, 197, 251
- Low B. C., 1980, *Solar Phys.*, 67, 57
- Meyer F., Schmidt H. U., Weiss N. D., 1977, *MNRAS*, 179, 741
- Nordlund A., Stein R. F., 1989, in: *Solar and Stellar Granulation*, Eds. R. J. Rutten & G. Severino, (Dordrecht: Kluwer), p. 453
- Nordlund A., Stein R. F., 1990, in: *IAU Symposium 138, Photosphere: Structure, Convection and Magnetic Fields*, Ed. J. O. Stenflo (Dordrecht: D. Reidel), p. 191
- Osherovich V. A., 1982, *Solar Phys.*, 77, 63
- Osherovich V. A., Flá T., 1983, *Solar Phys.*, 88, 109
- Osherovich V. A., Lawrence, 1983, *Solar Phys.*, 88, 117
- Pizzo V. J., 1986, *ApJ*, 302, 785
- Pizzo V. J., 1990, *ApJ*, 365, 764
- Proctor M. R. E., Weiss N. O., 1982, *Rep. Prog. Phys.*, 45, 1317
- Roberts B., Webb A. R., 1978, *Solar Phys.*, 56, 5
- Schmidt H. U., Wegmann R., 1983. In: *Dynamical problems in mathematical physics*, Ed. B. Brosowski & E. Martensen, Lang, Frankfurt, p. 137
- Schlüter A., Temesvary S., 1958, in: *IAU Symposium 6, Electromagnetic Phenomena in Cosmical Physics*, Ed. B. Lehnert (Cambridge University Press), p. 263
- Simon G. W., Weiss N. O., 1970, *Solar Phys.*, 13, 85
- Simon G. W., Weiss N. O., Nye A. H., 1983, *Solar Phys.*, 87, 65
- Skumanich A., Osherovich V., 1981, in: *The Physics of Sunspots*, Ed. L. E. Cram and J. H. Thomas (Sunspot: Sacramento Peak Observatory), p. 104
- Solov'ev A. A., 1982, *Soviet Astr.*, 26, 229
- Solov'ev A. A., 1983, *Astrophysics*, 19, 207
- Spruit H. C., 1977, Ph. D. thesis, University of Utrecht.
- Steiner O., Knölker M., Schüssler, M., 1994, in: *Solar Surface Magnetism*, Eds. R. J. Rutten & C. G. Schrijver, (Dordrecht: Kluwer), p. 441
- Steshenko N. V., 1967, *Izv. Krymsk. Ap. Obs.*, 37, 21
- Stone J. M., Norman M. L., 1992a, *ApJ Supp. Seri.*, 80, 753
- Stone J. M., Norman M. L., 1992b, *ApJ Supp. Seri.*, 80, 791
- Swarztrauber P. N., 1974, *SIAM Numer. Anal.*, 11, 1136
- Swarztrauber P. N., 1977, *SIAM Review*, 19, 490
- Syrovatskii S. I., Zhughzda Yu. D., 1967, *Sov. Astron.*, 11, 945
- Weiss N. O., Proctor M. R. E. 1981a/b, *J. Fluid Mech.*, 108, 247/273
- Winkler K. -H. A., Norman M. L., Mihalas D., 1984, *J. Quant. Spectrosc. Radiat. Transfer*, 31
- Yun H. S., 1970, *ApJ*, 162, 975
- Yun H. S., 1971, *Solar Phys.*, 16, 398